Continental Shelf Research, Vol. 10, No. 2, pp. 123–136, 1990.
Printed in Great Britain.

0278–4343/90 $3.00 + 0.00

Coupling between mixing and advection in a shallow sea front

DONG-PING WANG*, DAKE CHEN* and TOBY J. SHERWIN†

(*Received* 20 *April* 1989; *accepted* 14 *July* 1989)

Abstract—Tidal fronts in the Celtic Sea were numerically simulated for a 43 day period under realistic conditions of atmospheric and tidal forcing. In order to properly examine the boundary mixing we embedded a one-dimensional mixed-layer model into a three-dimensional general circulation model. Simulation from the embedded model shows generation of a tidal front that separates the well-mixed Irish Sea water from the stratified Celtic Sea water. The surface front does not respond to the spring–neap tidal variation, rather it is controlled mainly by the atmospheric forcing. During upwelling favorable winds the surface front moves with a southward Ekman transport and upwelling occurs at the edge of the tidally mixed water. Also, associated with the advancing surface front there is a prominent double-celled circulation. On the other hand, the surface front remains almost stationary during downwelling events. Model studies suggest that the atmospheric forcing plays an essential part of the thermocline evolution in shallow sea fronts.

INTRODUCTION

DEVELOPMENT of the thermocline in a water column is determined by flux of heat through the sea surface and by exchanges of heat with the adjacent water. In the past decade, there has been a steady progress towards a more complete understanding of the air–sea interaction in the open ocean (PRICE *et al.*, 1987). In particular, one-dimensional upper ocean thermal structure models are now quite realistic. There are two basic approaches in parameterization of the turbulent mixing; these include the bulk mixed-layer model which scales vertical entrainment to the wind stress frictional velocity, and the turbulence-closure model which relates vertical mixing to shear instabilities. Though these two model approaches are fundamentally different, both models give satisfactory prediction of the seasonal thermocline in the open ocean.

Application of mixed-layer models to the coastal ocean has not yet received much attention. Since transport processes in the coastal ocean are usually dominated by horizontal advections, it is generally assumed that a first-order description of the coastal circulation need not consider the effect of boundary mixing. On the other hand, the mixed-layer concept has been very useful in the study of thermocline development in tide-dominated waters. In particular, SIMPSON and HUNTER (1974) derived from the energy balance between surface heat flux and bottom tidal mixing, a simple yet powerful criterion for the formation of the thermocline. They found that there is a distinct boundary between

* Marine Sciences Research Center, The State University of New York, Stony Brook, NY 11794, U.S.A.
† Unit for Coastal and Estuarine Studies, University College of North Wales, Marine Science Laboratories, Menai Bridge, Anglesey, LL59 5EY, U.K.

well-mixed and stratified waters during spring and summer whose location can be determined from a critical number for $h\,u^{-3}$, where h is the water depth and u is the average tidal speed. BOWERS (1984) later extended the thermocline theory to include effects of wind mixing. CHEN *et al.* (1988) used a similar approach but with a turbulence-closure model, and they were also able to simulate the stratification cycle in Long Island Sound.

The one-dimensional mixed-layer model concept is useful in the study of stratification of a single water column. However, when horizontal advection becomes important, the one-dimensional approach may be less useful. For example, the energy balance model predicts large spatial variations of stratification over a spring–neap cycle, whereas observations indicated no such change in frontal positions (SIMPSON and BOWERS, 1981). Presumably, the advective processes somehow modify the appearance of tidal mixing. To study the coupled advective-mixing effect the one-dimensional model must be extended to at least include the cross-frontal dimension. For example, DE SZOEKE and RICHMAN (1981, 1984) examined effects of wind-induced mixing on coastal upwelling fronts by using a two-dimensional, two-layered model with bulk mixed-layer parameterization, and ADAMEC and GARWOOD (1985) studied the upper-ocean frontal processes by using an embedded, integral mixed-layer model. In this study we used an embedded mixed-layer model to simulate the response of tidal fronts in the Celtic Sea. Our approach is different from ADAMEC and GARWOOD (1985) in that we computed the mixed layer from a turbulence closure scheme and we used realistic atmospheric and tidal forcing conditions. Through numerical experiments effects of advection on thermal structures in shallow seas can be quantified.

MODEL FORMULATION

The general circulation model (GCM) used in this study is a three-dimensional, primitive-equation model of WANG (1987). We consider only a two-dimensional balance in this study; the along-frontal gradients are set to zero. While there is no fundamental difficulty in modelling the three-dimensional processes, the two-dimensional model results are easier to analyse. The equations of motion, the thermodynamic equation, and the equation of continuity are

$$\frac{Du}{Dt} - fv = -\frac{\partial P}{\partial x} + \frac{\partial}{\partial z}\left(A_v \frac{\partial u}{\partial z}\right) \tag{1}$$

$$\frac{Dv}{Dt} + fu = \frac{\partial}{\partial z}\left(A_v \frac{\partial v}{\partial z}\right) \tag{2}$$

$$O = -\frac{\partial P}{\partial z} + \rho g \tag{3}$$

$$O = \frac{\partial u}{\partial x} + \frac{\partial w}{\partial z} \tag{4}$$

$$\frac{DT}{Dt} = \frac{\partial}{\partial z}\left(K_v \frac{\partial T}{\partial z}\right) \tag{5}$$

$$\rho = \rho_o + \beta T, \tag{6}$$

where $D/Dt = \partial/\partial t + u\partial/\partial x + w\partial/\partial z$, and u,v, and w are cross-channel, along-channel, and vertical velocities, T is temperature, f is the Coriolis parameter, P is pressure, ρ is density, β is a thermal expansion constant, A_v is vertical viscosity coefficient, and K_v is vertical diffusivity coefficient. Horizontal diffusive terms are not listed in equations (1) and (2), although they are included in numerical simulations using a small horizontal eddy coefficient of 10^5 cm^2 s^{-1}. Analysis of model results indicated that the horizontal dissipation has negligible contribution to the momentum balance.

The eddy coefficients are computed from the Munk–Anderson scheme,

$$A_v = A_o(1 + 10\,R_i)^{-0.5} \tag{7a}$$

$$A_v = K_o(1 + 3.3\,R_i)^{-1.5}, \tag{7b}$$

where $A_o = 100\,\text{cm}^2\,\text{s}^{-1}$, $K_o = 10\,\text{cm}^2\,\text{s}^{-1}$, and R_i is the gradient Richardson number. The boundary conditions follow WANG (1987); these include surface wind stress and heat flux, quadratic bottom friction, and slip sidewall. Equations (1)–(7) form a complete GCM which together with initial conditions and external forcing will compute the frontal circulation. Previously, JAMES (1978) and WANG (1984) studied the two-dimensional frontal adjustment based on this set of equations.

The GCM with Munk–Anderson scheme, however, does not properly simulate the rapid and sharp variations of the mixed-layer depth. It is necessary to use a mixed-layer model for realistic representation of the boundary layer structure. In this study the mixed-layer model is from CHEN *et al.* (1988) which is an extension of MELLOR and DURBIN (1975). The eddy coefficients according to the closure scheme are

$$A_v = L\,q\,S_M \tag{8a}$$

$$K_v = L\,q\,S_H, \tag{8b}$$

where S_H and S_M are functions of Richardson number; if $R_i > 0.23$, $S_H = S_M = 0$. In other words, turbulence is completely suppressed below the mixed layer where Richardson numbers >0.23. In equation (8), L is a length scale, and q^2 is twice the turbulent kinetic energy. A level 2 closure scheme is used which assumes local balance of turbulence energy production and dissipation. The mixed-layer model includes both wind and tidal mixing; a logarithmic velocity layer is assumed at the surface and at the bottom, and the asymptotic length scale is determined by the ratio of the first to the zero moment of q in the mixed layer. A simple criterion is used to allow merger of upper and bottom boundary layers (CHEN *et al.*, 1988).

In the mixed-layer model vertical shears are generated by surface wind stress and bottom tidal stress. The vertical temperature (density) profiles also are needed for evaluation of the Richardson number and for use in the turbulence energy equation. In the one-dimensional model approach temperatures are computed from the vertical diffusion equation. However, this approach is not adequate when horizontal advections are important. To resolve this difficulty we embedded the mixed-layer model into the GCM. Temperatures for the mixed-layer model are obtained from results of the GCM which uses the complete advective and diffusive equation. Given the temperature profile the one-dimensional mixed-layer model is complete. On the other hand, the mixed-layer structure, or specifically the mixed-layer eddy coefficients, must transmit to the GCM. In other words, eddy coefficients used in the GCM (equations 1, 2 and 5) must reflect the boundary-layer structure. This is accomplished through replacing eddy coefficients computed from

the Munk–Anderson scheme (equation 7) by those from the mixed-layer model, if the latter have larger numerical value. In practice, since eddy coefficients computed from the mixed-layer model have a sharp cutoff immediately below the mixed-layer depth, our method adds surface and bottom boundary layers to the general circulation model without modifying the interior structure.

Because the one-dimensional, mixed-layer model can be calculated independent of the three-dimensional GCM, there is no need to fully resolve boundary structure in the GCM. Also, because the GCM only responds to the variation of mixed-layer depth, the GCM calculation is not sensitive to the detailed prediction of the mixed-layer dynamics. An alternative approach to the embedded mixed-layer model is to completely replace the Munk–Anderson scheme in the GCM by the turbulence closure scheme, which will be similar to BLUMBERG and MELLOR (1987). Model tests indicated that these two approaches give similar results under idealized forcing. However, the numerical stability of these two approaches is quite different under realistic forcing. Eddy coefficients below the mixed layer will remain finite with the embedded mixed-layer model when there are remnant vertical shears. On the other hand, eddy coefficients will immediately become zero (or, a small background value) with the other approach, and the GCM may become unstable during wind relaxations when the upper mixed layer suddenly disappears.

MODEL CONFIGURATION: CELTIC SEA TIDAL FRONT

Tidal currents are about 30 cm s^{-1} on the Celtic Sea outer shelf and about 100 cm s^{-1} in the Irish Sea. Because of the large difference in tidal mixing, water is well-mixed in the Irish Sea and is stratified in the Celtic Sea. There is a clearly defined tidal front at the northern end of the Celtic Sea which separates the cool Irish Sea water from the warm Celtic Sea water. To study the two-dimensional front the embedded mixed-layer model is oriented along the axis of St. George's Channel (Fig. 1). The model has a horizontal dimension of 300 km with a horizontal resolution of 10 km, and a constant water depth of

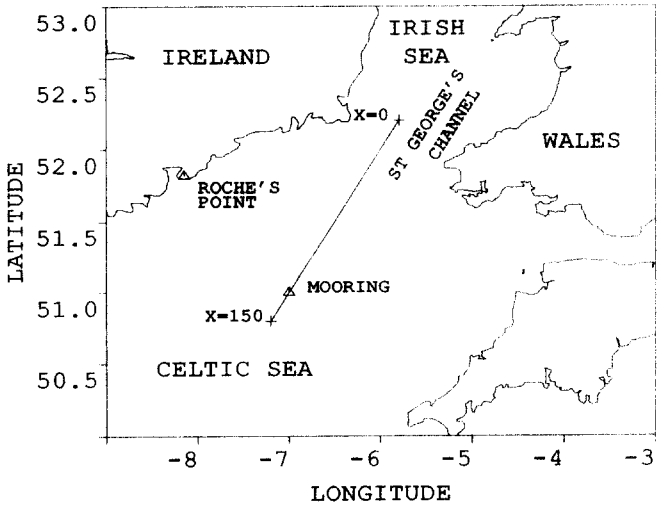

Fig. 1. The northern Celtic Sea showing the mooring location.

90 m with vertical resolutions of 10 m in the GCM and 5 m in the mixed-layer model. The northern end of the model which extends well into the Irish Sea is closed in order to simulate effects of the constricted Irish Sea. The southern end of the model which is placed well beyond the region of interest is open. A simple advective boundary condition for temperature is used at the open end (WANG, 1987).

Tidal current distribution in the model is obtained from the numerical tidal model results of PINGREE and GRIFFITHS (1978). The semidiurnal (M_2) current is 100 cm s^{-1} in the Irish Sea ($x < 0$, Fig. 1), 30 cm s^{-1} in the open Celtic Sea ($x > 90$ km, Fig. 1), and in between the velocity changes linearly. The model also includes the S_2 tide whose amplitude is everywhere equal to 30% of the M_2 tide. A combination of the two semidiurnal tidal components results in a spring–neap ratio of about 1.8. The spatially varying tidal currents are specified point-by-point in the one-dimensional mixed-layer model, which results in the differential tidal mixing along St. George's Channel. On the other hand, because the tidal excursion length (<10 km) is small compared to the horizontal advective scale, tidal currents are not modeled in the GCM. In other words, for tidal motion only the effect of mixing is considered in the embedded model.

The atmospheric forcing includes wind stress and heat flux. The simulation period is 43 days from Julian day 158 (8 June) to day 201 (21 July), 1984. Standard atmospheric observations were obtained at a weather station at Roche's Point (Fig. 1). Wind stress was computed from measured wind using a drag coefficient of 1.3×10^{-3}. The solar radiation

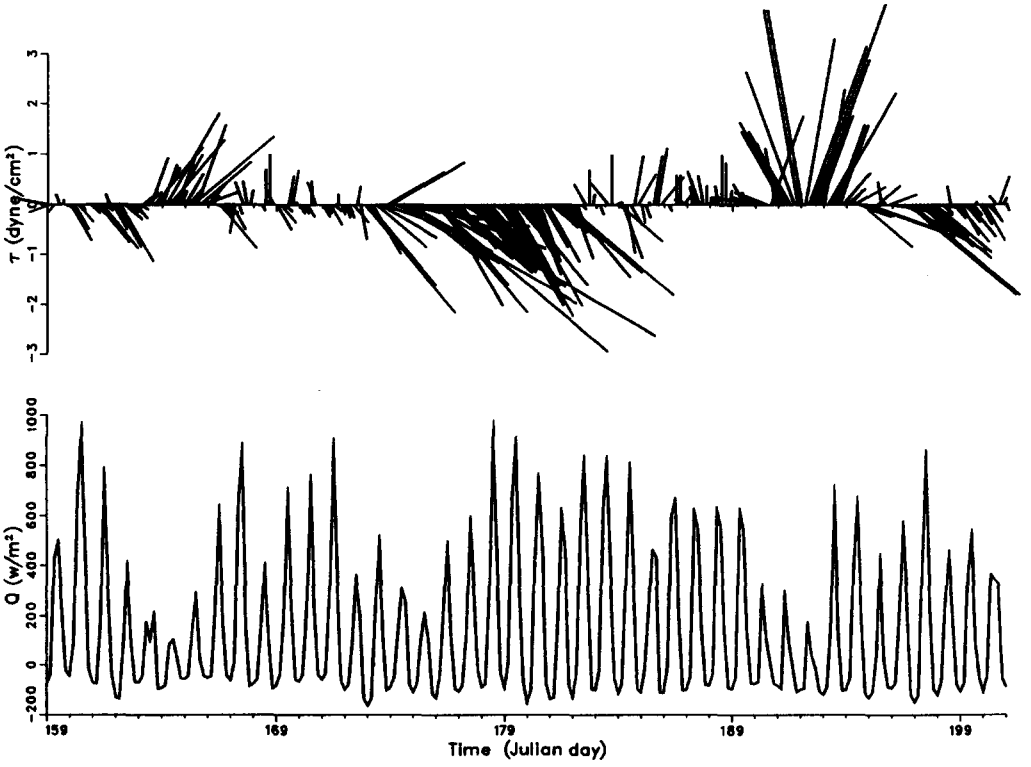

Fig. 2. The wind stress and heat flux data at Roche's Point.

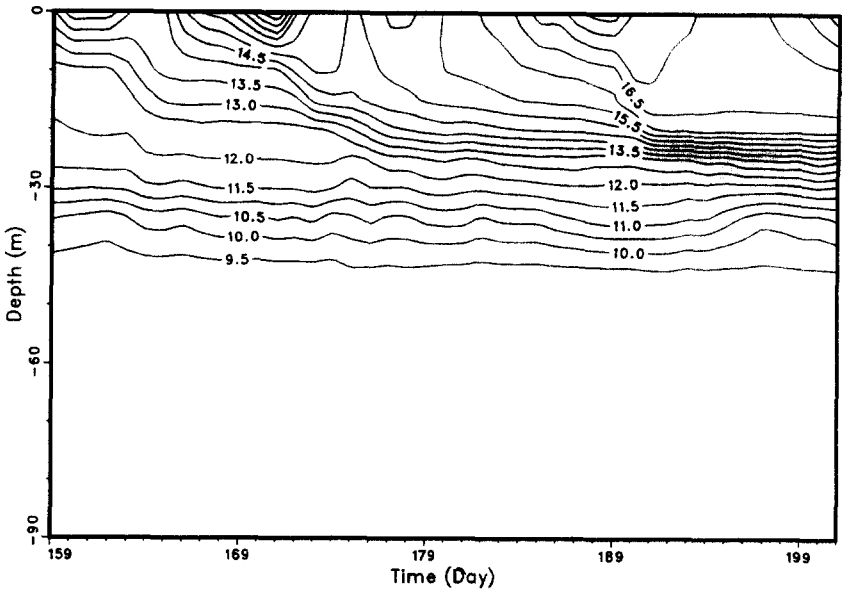

Fig. 3. Temperature (°C) at the mooring location.

was measured, and the sensible and latent heat fluxes were calculated using bulk formula from observed air and sea surface temperatures. The heat fluxes are specified in the model's surface boundary condition, and hence, there is no feedback in the model between air and ocean. Figure 2 shows time series of wind stress and heat flux for the study period. Water temperatures were collected with thermistor chains at an open-shelf site (Fig. 1) about 100 km south of the Irish Sea entrance (SHERWIN, 1986). Figure 3 shows the observed daily averaged temperature time series. The record indicated a general warming trend in the upper 30 m. There were also marked stratification changes in the upper ocean, for example, a shallow thermocline developed around days 170 and 190. Comparison between water temperature and atmospheric data (Fig. 2) suggests that the upper-ocean thermal structure was strongly influenced by wind forcing.

The water column initially is assumed to have a two-layered structure: the upper layer is 12°C, the lower layer 9°C, and the interface is at 30 m depth. This initial temperature profile is adjusted by running the one-dimensional mixed-layer model with observed wind and tide for 5 days. The new temperature profiles, which are similar to the observed temperature transect (SHERWIN, 1988), are used for the initial condition. The initial flow field is a geostrophic current which, however, is weak (<1 cm s^{-1}).

MODEL RESULTS

Model simulation is run for 43 days starting from Julian day 158 (8 June) 1984. For clarity, we only show model results on a 150 km subsection from the southern entrance of the Irish Sea ($x = 0$) to the open Celtic Sea ($x = 150$ km). Solutions for $x < 0$ are similar to that at $x = 0$, and solutions for $x > 150$ km are similar to that at $x = 150$ km. Figure 4a–c shows temperature contours at surface, 20 m and 40 m depths; below 40 m, temperatures are uniform. The location of the surface front is defined as the southern boundary of the

well-mixed water (Fig. 4a). The surface front starts at $x = 20$ km, and advances southward to $x = 50$ km during the first week; afterwards, the surface front fluctuates, but does not move back to $x < 50$ km. The bottom front which is marked by the 10°C contour, stays at $x = 50$ km (Fig. 4c). At $x = 50$ km the M_2 tidal current is 60 cm s^{-1}, corresponding to $\log (h/C_D u^3) = 1.6$ (in cgs unit). For comparison, the Simpson–Hunter criterion yields an empirical constant of 1.5. Clearly, the mean frontal position calculated by the model is quite good. We noted that despite a 6-fold change in u^3 between spring and neap tides the

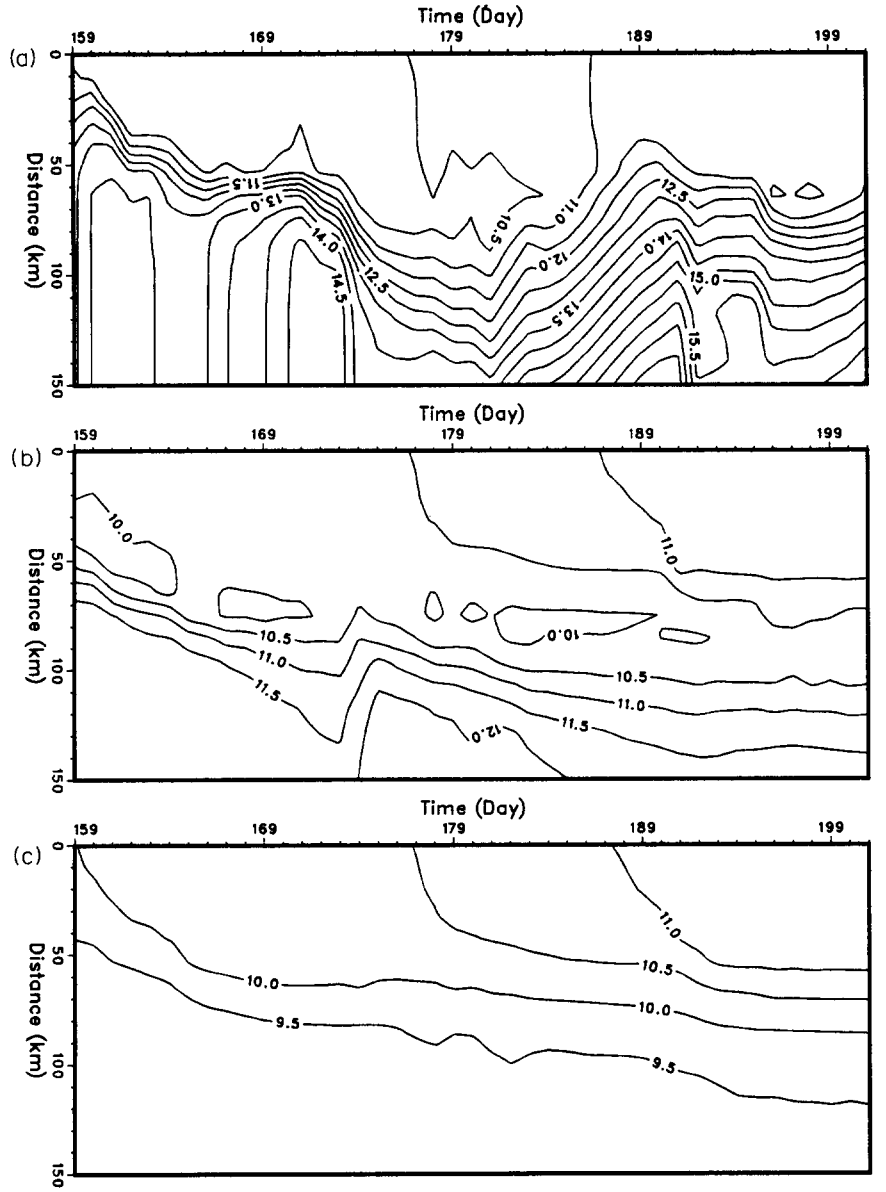

Fig. 4. Temperature (°C) at (a) surface, (b) 20 m depth and (c) 40 m depth.

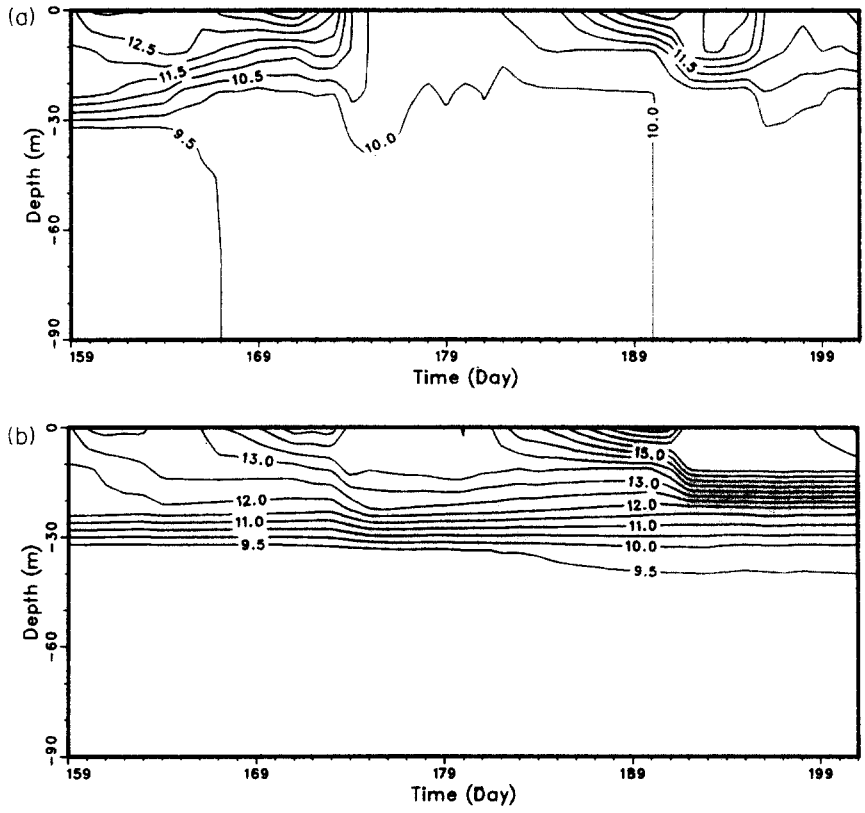

Fig. 5. Temperature (°C) at (a) x = 70 km and (b) x = 140 km.

frontal position shows no spring–neap modulation (spring tides occur at days 165, 180 and 194).

Surface temperature shows large spatial and temporal variations. Between days 159 and 173 there is a sharp transition zone of less than 20 km wide between the cool Irish Sea water and the warm open-shelf water. However, from day 174 the front starts advancing rapidly to the south and the transition zone broadens considerably to about 50 km wide. The temperature transition zone remains very broad even after the front retreats. The temperature structure at intermediate depth also is interesting. Figure 4b shows temperature contours at 20 m depth. There is little resemblance between surface and mid-depth temperature structures, indicating that the warm surface water is mostly confined to the shallow mixed layer. Also, between the cool well-mixed water and the warm stratified water there is a distinct band of cold water of about 10°C. This anomalously cold water must come from the lower layer through upwelling (vertical advection) or entrainment (growth of the lower mixed layer).

Figure 5a and b shows time history of temperature structures at x = 70 km and x = 140 km. Far from the front (x = 140 km), the temperature change is typical of the upper-ocean response. The thermocline is stronger during weak winds such as at days 170 and 190, while it is rapidly eroded during storms such as at days 175 and 192. The predicted thermocline evolution agrees well with the thermistor chain data (Fig. 3). The temperature time series

near the front, on the other hand, shows strong effects of horizontal advection. For example, the stratification at $x = 70$ km suddenly breaks down on day 175, which is much more drastic than the similar event at $x = 140$ km. Since atmospheric forcing is the same at both locations, the difference in upper-ocean response between these two locations must attribute to effects of the horizontal advection.

The relation between wind forcing and horizontal advection is examined. Figure 6a shows the time–depth plot of the daily averaged, cross-frontal velocity at $x = 70$ km. It is necessary to show the filtered (daily averaged) time series since instantaneous velocities are masked by strong inertial currents. During the first wind episode on day 173 a northwesterly wind drives a southward Ekman transport in the upper layer and a northward return flow below the thermocline. This cross-frontal circulation leads to a rapid southward advance of the surface front (Fig. 4a). A similar response is found during the third episode of a modest northwesterly wind on day 196. In contrast, during the second wind episode on day 190 a southerly wind drives a strong northward surface current along the direction of the wind, but the surface front remains stationary.

The response of the surface front to a northwesterly wind is strikingly different from that to a southerly wind. This difference is the consequence of coupling between horizontal

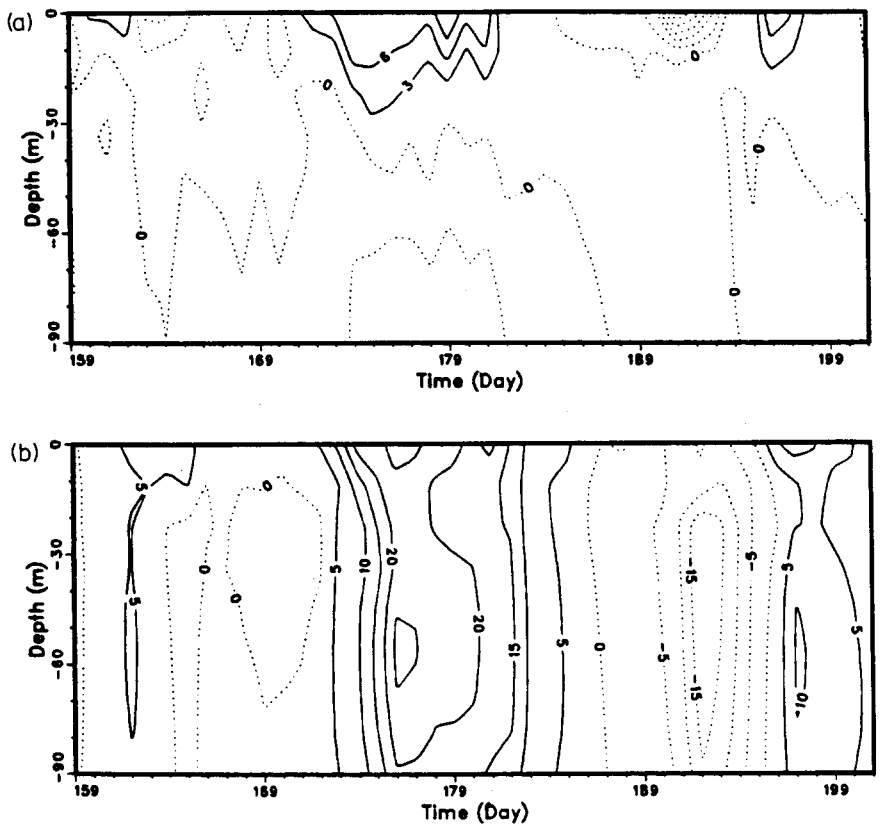

Fig. 6. Daily averaged cross-channel current and (b) daily averaged along-frontal current at $x = 70$ km.

advection and vertical mixing. When the surface flow is southward, advection of cold water reduces vertical stability in the upper layer, which enhances vertical mixing. In the extreme case convective mixing may take place. The feedback between southward advection and vertical mixing therefore is effective. This leads to the rapid reduction of surface temperature and an apparent southward intrusion of cool water. The rapid deepening of the mixed layer on day 175 (Fig. 5a) and the advance of the surface front between days 159 and 162 (Fig. 4a) are examples of reinforced mixing and advection. In contrast, when the surface current is northward, advection of warm water is counteracted by vertical mixing (entrainment of cold water); consequently, there is only a small change of surface temperature during southerly wind episodes.

Figure 6b shows the time–depth plot of the daily averaged, along-frontal currents at x = 70 km. The along-frontal currents are homogeneous below the upper mixed layer, indicating that they are geostrophic currents associated with sea surface slope. During a northwesterly wind episode the southward Ekman transport lowers sea level in the Irish Sea and the geostrophic flows are eastward with maximum currents of about 30 cm s^{-1}. During a southerly wind episode the wind set-up produces higher sea level in the Irish Sea and the geostrophic flows are westward with maximum currents of about 20 cm s^{-1}. For comparison, the mean baroclinic geostrophic current, which has a maximum current at the base of the tidal front, is about 5 cm s^{-1} (westward). Thus, the along-frontal motion is dominated by wind-driven barotropic currents. In the upper Ekman layer the along-frontal currents have strong vertical shears. For example, on day 192 a southerly wind drives an eastward Ekman current against a prevailing westward slope current, causing a much weaker current in the surface.

Strong upwelling (flow divergence) often occurs along the front during northwesterly winds. Figure 7a and b shows temperature cross-sections on days 173 and 177. The surface front on day 173 is located at x = 50 km and the thermocline is shallow. However, on day 177 after the onset of a major northwesterly storm the front has advanced to x = 80 km, a deep mixed layer appears, and the well-mixed Irish Sea water is separated from the stratified Celtic Sea water by a dome of cold upwelled water. Figure 8a and b shows corresponding cross-frontal circulation (stream function). The surface flow is a southward Ekman current; the magnitude of Ekman transport is tripled on day 177 as the strength of the storm picks up. The lower-layer flow is a return flow which compensates the Ekman transport. The streamline distribution, however, is not uniform. Most noticeably, there is a strong recirculation, or, upwelling, at the edge of the tidally mixed water. This cross-frontal circulation pattern is consistent with the cold-dome temperature structure.

To examine more closely the recirculation pattern, we remove a reference value (stream function at x = 0) from the stream functions (Fig. 9a, b). Since vertical velocity is not affected by differencing, the relative stream function shows the recirculation pattern more clearly. On day 173 the secondary recirculation is confined entirely to the upper stratified layer and the tidally mixed water seems to act like a barrier to the Ekman transport. This recirculation pattern is caused by the sharp change of mixed-layer depths across the tidal front. The mixed layer is deep in $x < 50$ km, but, is almost non-existent in $x > 50$ km. Since the Ekman velocity shears are much stronger in the shallow mixed layer than in the well-mixed water, the surface flow is also stronger in the shallow mixed layer. Consequently, there is a surface flow divergence at the edge of the tidally mixed water (x = 50 km). The upper-layer transport in the tidally mixed water also is smaller than in the stratified water, which futher contributes to the upwelling. In coastal water the Ekman transport is reduced

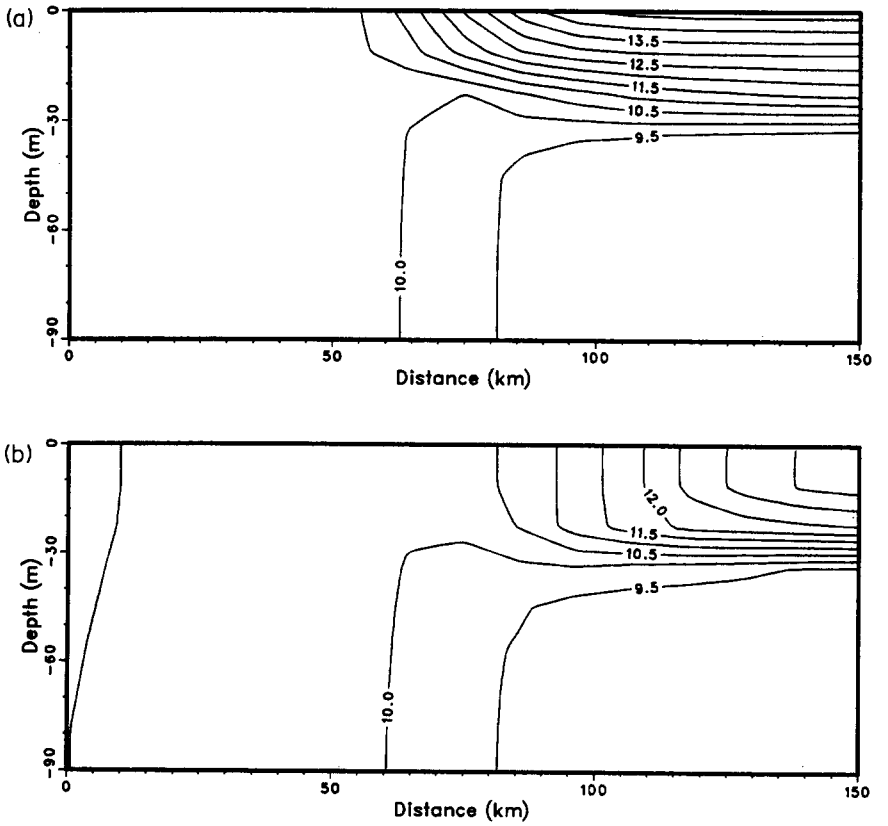

Fig. 7. Temperature (°C) cross-sections at (a) t = 173 day and (b) t = 177 day.

by a uniform return flow such that the total cross-shore transport is zero. Thus, the upper-layer transport is smaller with a deeper mixed layer.

On day 177 the surface front moves southward to x = 80 km (Fig. 6b). Strong upwelling is still present at the edge of the tidally mixed water. There is also a secondary upwelling ahead (at the south side) of the surface front. Between these two upwelling zones there is a pronounced downwelling zone at the front. This cross-frontal, double-celled circulation pattern is remarkably similar to the one proposed by MOOERS *et al.* (1976) for coastal upwelling. The complex recirculation pattern is associated with the spatial variation of mixed-layer depths. The mixed layer is shallow in the cold dome (between the edge of well-mixed water and the surface front) because of intense upwelling. However, advection of cold water towards the surface front leads to convective mixing, resulting in an anomalous deepening of the mixed layer (Fig. 7b). Thus, a flow convergence is formed at the front. Ahead of the front the mixed layer is only affected by the entrainment and is shallower than the mixed layer at the front. Thus, a flow divergence is formed ahead of the front. Upwelling at the edge of tidally mixed water also is enhanced by an increase of the upper-layer transport. The secondary recirculation is manifest of a similar, but somewhat singular-behaved process described in the analytical theory of DE SZOEKE and RICHMAN (1984).

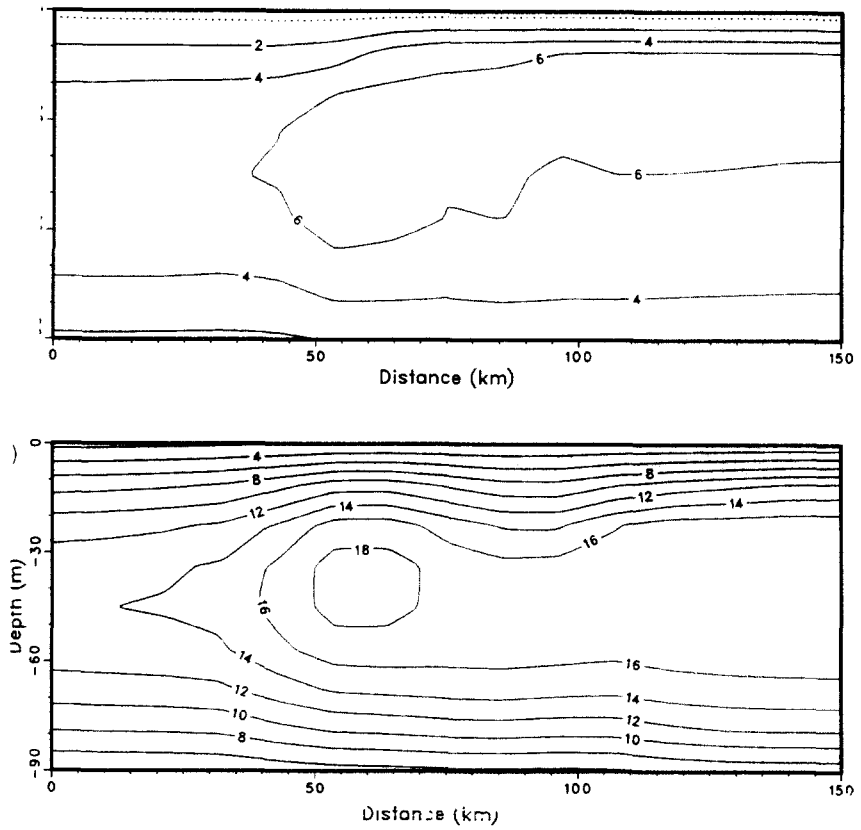

Fig. 8. Stream functions (in arbitrary unit) at (a) t = 173 day and (b) t = 177 day.

DISCUSSION

Model simulation using observed wind, heat flux and tidal current indicates that frontal movements are mainly controlled by the northwesterly winds. When the Ekman transport brings cool water across the front, the thermocline can be quickly eroded even with a modest wind stirring. The importance of coupling between advection and mixing in the coastal ocean is highlighted by the contrast in thermocline evolution between near the front and in the open ocean (Fig. 5a,b). The model study also indicates that strong upwelling takes place during northwesterly winds along the edge of the tidally mixed water. Furthermore, as the surface front moves offshore (southward) a strong convergence zone develops behind the front. The predicted double-cell circulation seems to compare favorably well with the frequent observations of two foam lines in the tidal front, a temperature minimum zone between well-mixed water and stratified water and a slick line in the region of the maximum temperature gradient (SIMPSON *et al.*, 1978). The temperature minimum zone may be identified with the doming of cold water and the slick line with the convergence zone at the front.

Our study indicates a mean (density-driven) baroclinic current of about 5 cm s^{-1} which is substantially smaller than transient wind-driven barotropic currents. (The mean circu-

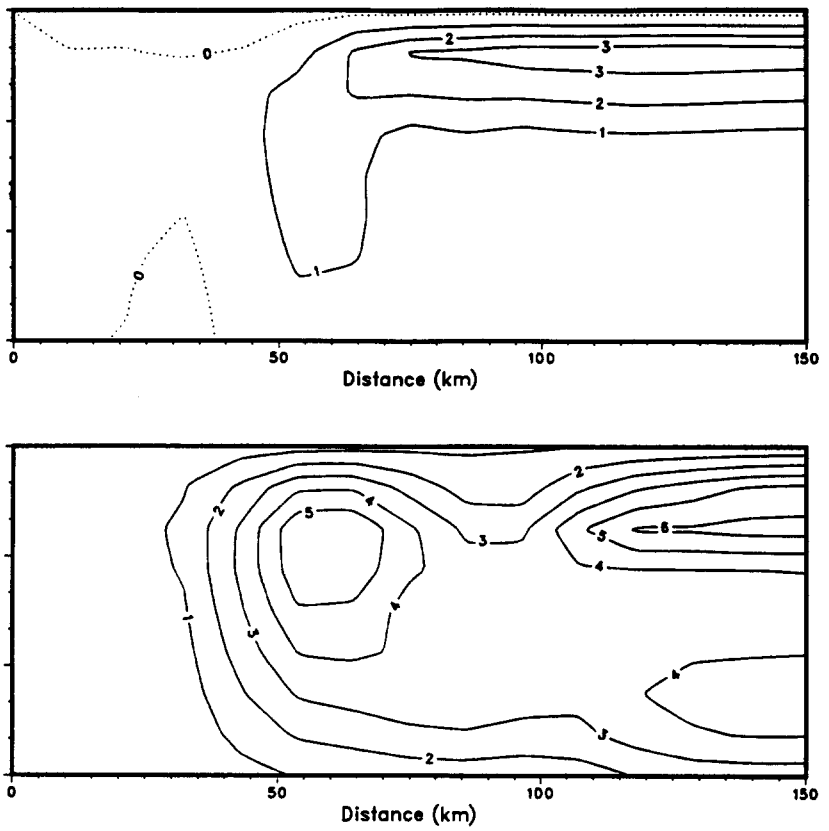

Fig. 9. Relative stream functions (in arbitrary unit) at (a) t = 173 day and (b) t = 177 day.

lation is obtained by running the model with mixing only.) This may explain the lack of observational evidence of the along-frontal jet predicted by some earlier studies (SIMPSON *et al.*, 1978). The mean cross-frontal velocity is even weaker, less than 1 cm s^{-1}. It seems unlikely that the observed frontal convergence can be associated with the mean circulation. The baroclinic jet, however, may become significant in late summer when there is a greater thermal gradient. The model study also indicates that the frontal position does not correlate with the spring–neap cycle. Tidal mixing in $x > 50$ km appears to be completely overwhelmed by wind-driven advection and mixing. The SIMPSON and HUNTER (1974) criterion only defines the boundary of the tidally mixed water.

Previously, use of the embedded mixed-layer models has focused on idealized atmospheric forcing. However, since formation of mixed layers depends sensitively on the time history of atmospheric forcing, it is difficult to construct a truly representative forcing function. By using observed forcing data we are able to produce an ensemble of episodes through which the significance of vertical mixing can be realized. Model results indicate that the sea surface temperature distribution (Fig. 4a) is a complex function of heating, advection and mixing. While movements of the front generally follow the direction of current, there is no linear relation between the magnitude of surface flow and the isotherm displacement. Also, because the mixed-layer depth does not stay constant, the horizontal

pressure gradient (the geostrophic current) cannot be readily obtained from surface temperature distribution. In order to take full advantage of the satellite remote sensing (the SST data), numerical experiments with the advective-mixing model are required to determine the proper conditions for extrapolation.

Acknowledgements—This work was initiated when DPW was a summer guest investigator with the Unit for Coastal and Estuarine Studies, University College of North Wales. He thanks the hospitality of Dr Alan Elliott and Prof. John Simpson. The model computation was supported by the Cornell National Supercomputer Facilities. This work was supported by the Institute for Naval Oceanography (DPW) and the Admiralty Research Establishment (TJS). This is MSRC Contribution no. 704.

REFERENCES

ADAMEC D. and R. W. GARWOOD (1985) The simulated response of an upper-ocean density front to local atmospheric forcing. *Journal of Geophysical Research*, **90**, 917–928.

BLUMBERG A. F. and G. L. MELLOR (1987) A description of a three-dimensional coastal circulation model. In: *Three-dimensional coastal ocean models*, N. S. HEAPS, editor, American Geophysics Union, pp. 1–17.

BOWERS D. G. (1984) A two layer model of the seasonal thermocline and its application to the Celtic Sea. UCES Report U84-4. University College of North Wales.

CHEN D., S. G. HORRIGAN and D.-P. WANG (1988) The late summer vertical nutrient mixing in Long Island Sound. *Journal of Marine Research*, **46**, 753–770.

DE SZOEKE R. A. and J. G. RICHMAN (1981) The role of wind-generated mixing in coastal upwelling. *Journal of Physical Oceanography*, **11**, 1534–1547.

DE SZOEKE R. A. and J. G. RICHMAN (1984) On wind-driven mixed layers with strong horizontal gradients—a theory with application to coastal upwelling. *Journal of Physical Oceanography*, **14**, 364–377.

JAMES I. D. (1978) A note on the circulation induced by a shallow sea front. *Estuarine, Coastal and Marine Science*, **7**, 197–202.

MELLOR G. L. and P. A. DURBIN (1975) The structure and dynamics of the ocean surface mixed layer. *Journal of Physical Oceanography*, **5**, 718–728.

MOOERS C. N. K., C. A. COLLINS and R. L. SMITH (1976) The dynamic structure of the frontal zone in the coastal upwelling region. *Journal of Physical Oceanography*, **6**, 3–21.

PINGREE R. D. and D. K. GRIFFITHS (1978) Tidal fronts on the shelf seas around the British Isles. *Journal of Geophysical Research*, **83**, 4615–4622.

PRICE J. F., E. A. TERRAY and R. A. WELLER (1987) Upper ocean dynamics. *Reviews of Geophysics*, **25**, 193–203.

SHERWIN T. (1986) Current velocities and water temperatures in the Celtic Sea, summer 1984. UCES Report U86-1, University College of North Wales.

SIMPSON J. H. and J. R. HUNTER (1974) Fronts in the Irish Sea. *Nature*, **250**, 404–406.

SIMPSON J. H. and D. G. BOWERS (1981) Models of stratification and frontal movement in shelf seas. *Deep-Sea Research*, **28**, 727–738.

SIMPSON J. H., C. M. ALLEN and N. C. G. MORRIS (1978) Fronts on the continental shelf. *Journal of Geophysical Research*, **83**, 4607–4614.

WANG D.-P. (1984) Mutual intrusion of a gravity current and density front formation. *Journal of Physical Oceanography*, **14**, 1191–1199.

WANG D.-P. (1987) The strait surface outflow. *Journal of Geophysical Research*, **92**, 10807–10825.